Gabriel Zada
M. Beatriz S. Lopes
Srinivasan Mukundan Jr.
Edward R. Laws Jr.
Editors

Atlas of Sellar and Parasellar Lesions

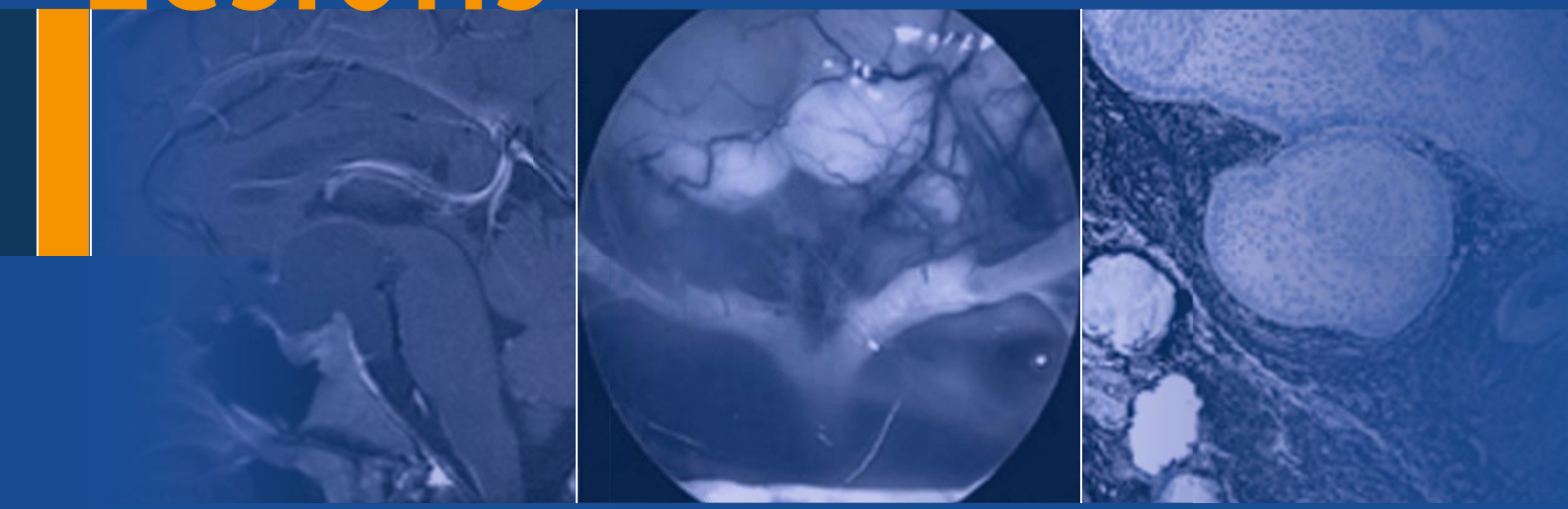

Clinical, Radiologic, and Pathologic Correlations

Springer

Atlas of Sellar and Parasellar Lesions

Gabriel Zada • M. Beatriz S. Lopes
Srinivasan Mukundan Jr. • Edward R. Laws Jr.
Editors

Atlas of Sellar and Parasellar Lesions

Clinical, Radiologic, and Pathologic Correlations

Springer

Editors
Gabriel Zada
Department of Neurosurgery
University of Southern California
Los Angeles, CA
USA

M. Beatriz S. Lopes
Department of Pathology
University of Virginia
Charlottesville, VA
USA

Srinivasan Mukundan Jr.
Department of Radiology
Brigham and Women's Hospital
Boston, MA
USA

Edward R. Laws Jr.
Department of Neurosurgery
Brigham and Women's Hospital
Boston, MA
USA

ISBN 978-3-319-22854-9 ISBN 978-3-319-22855-6 (eBook)
DOI 10.1007/978-3-319-22855-6

Library of Congress Control Number: 2015953343

Springer Cham Heidelberg New York Dordrecht London

Printed on acid-free paper

Springer International Publishing AG Switzerland is part of Springer Science+Business Media (www.springer.com)

We would like to dedicate this atlas to the many gifted teachers and physicians on whose shoulders we have stood and in particular to Dr. Harvey Cushing, who laid the foundation for this work. We would also like to dedicate this atlas to our patients, who have equally taught and inspired us.

Preface

The sella turcica and parasellar area are rich and intricate anatomic regions of the intracranial cavity. They form a unique spatial confluence of numerous key anatomic and physiologic systems. The normal anatomic organization and functional integrity of the important structures contained within this small space may be easily distorted by any number of diverse pathological processes arising in and around this region. For this reason, patients presenting with diseases of the sellar and parasellar region may seek the expertise of numerous medical practitioners, including family practitioners, neurologists, ophthalmologists, otolaryngologists, endocrinologists, and neurosurgeons, among many others. In addition, optimization of treatment for patients with pituitary disease and other lesions of the sellar and parasellar region is best provided by a multidisciplinary team comprised of these very specialties, with the assistance of neuroradiologists, radiation oncologists, neuro-oncologists, neuropathologists, and others. The spectrum of disease arising in the sellar region ranges from functional pituitary adenomas causing hormonal excess syndromes such as acromegaly or Cushing's disease, to a variety of cystic lesions, to metastatic or other malignant tumors, infections, inflammatory diseases, and vascular lesions, among many others. The assortment of entities presenting in this small yet immensely critical region is as diverse as anywhere else in the human body.

After treating many patients with sellar lesions, one begins to develop a sense for both the typical features and uniqueness of each patient and his or her disease, with regard to the clinical presentation, anatomic features, imaging characteristics, and pathology. Fortunately, patterns in the clinical presentation and underlying disease processes do emerge and can be used to understand the disease process and to optimally treat patients. An understanding of the endocrinologic, visual, and neurologic features of processes occurring in this region is paramount to diagnosing sellar and parasellar lesions and managing these patients. Similarly, a thorough understanding of the anatomic relationships among the pituitary gland, infundibulum, optic chiasm and nerves, internal carotid arteries, cranial nerves, hypothalamus, and third ventricle is mandatory. Our collective ability to effectively manage the variety of sellar and parasellar pathology has evolved tremendously over the past three decades, resulting from the development of many technological advances, including improved imaging modalities, radioimmunoassay techniques, hormone replacement therapy, the operative microscope and microsurgical technique, endoscopic neurosurgery, and radiosurgery.

Most cases in this atlas have been collected over the senior author's experience of over three decades of treating patients with sellar and parasellar disease. Traversing the sphenoid sinus more than 5000 times in order to treat patients with a wide spectrum of sellar and parasellar lesions has led to a deep appreciation for the amazing catalogue of findings possible in this region. It is our hope that the cases, images, and clinical and operative "pearls" in this atlas will

convey a sense of marvel for the intricacy of this region of the body and will impart the benefit of our experience in precisely accessing this region surgically, improving the lives of patients with the many types of pathologic processes occurring here.

Los Angeles, CA, USA — Gabriel Zada, MD, MS
Charlottesville, VA, USA — M. Beatriz S. Lopes, MD, PhD
Boston, MA, USA — Srinivasan Mukundan Jr., PhD, MD
Boston, MA, USA — Edward Laws Jr., MD

Acknowledgments

This work could not have been accomplished without the same kind of multidisciplinary approach that we utilize clinically. With the assistance of so many experts from a variety of perspectives and roles, we have been successful. Those involved include our office and medical assistants, our nurses, nurse practitioners and physician assistants, our residents and fellows, and so many of our medical and surgical colleagues.

Particular mention goes to Dr. Raymond Huang, who was essential in creating the imaging segments; Dr. Kyle Hurth who helped with selected pathology images; Dr. Eric Ojerholm who collated and organized the case material; and Lee Klein from Springer who masterfully coordinated the production of this atlas.

Contents

Contributors

Paolo Cappabianca, MD Division of Neurosurgery, Department of Neurosciences, Reproductive and Odontostomatological Sciences, Universita' degli Studi di Napoli Federico II, Naples, Italy

John D. Carmichael, MD Division of Endocrinology and Diabetes, Department of Medicine, University of Southern California Pituitary Center, Los Angeles, CA, USA

Luigi Maria Cavallo, MD, PhD Division of Neurosurgery, Department of Neurosciences, Reproductive and Odontostomatological Sciences, Universita' degli Studi di Napoli Federico II, Naples, Italy

Ching-Jen Chen, MD Department of Neurosurgery, University of Virginia Health System, Charlottesville, VA, USA

Dale Ding, MD Department of Neurosurgery, University of Virginia, Charlottesville, VA, USA

Ian F. Dunn, MD Department of Neurosurgery, Brigham and Women's Hospital, Boston, MA, USA

Raymond Y. Huang, MD, PhD Department of Radiology, Brigham and Women's Hospital, Boston, MA, USA

Edward Laws Jr , MD Department of Neurosurgery, Brigham and Women's Hospital, Boston, MA, USA

M. Beatriz S. Lopes, MD, PhD Department of Pathology (Neuropathology), University of Virginia School of Medicine, Charlottesville, VA, USA

Joshua W. Lucas, MD Department of Neurosurgery, Keck School of Medicine, University of Southern California, Los Angeles, CA, USA

Srinivasan Mukundan Jr , PhD, MD Department of Radiology, Brigham and Women's Hospital, Boston, MA, USA

Miriam Padilla, MD Division of Endocrinology and Diabetes, Department of Medicine, University of Southern California Pituitary Center, Los Angeles, CA, USA

Jason Sheehan, MD, PhD Department of Neurosurgery, University of Virginia, Charlottesville, VA, USA

Domenico Solari, MD, PhD Division of Neurosurgery, Department of Neurosciences, Reproductive and Odontostomatological Sciences, Universita' degli Studi di Napoli Federico II, Naples, Italy

Teresa Somma, MD Division of Neurosurgery, Department of Neurosciences, Reproductive and Odontostomatological Sciences, Universita' degli Studi di Napoli Federico II, Naples, Italy

Robert M. Starke, MD Department of Neurosurgery, University of Virginia, Charlottesville, VA, USA

Alessandro Villa, MD Division of Neurosurgery, Department of Neurosciences, Reproductive and Odontostomatological Sciences, Universita' degli Studi di Napoli Federico II, Naples, Italy

Gabriel Zada, MD, MS Department of Neurological Surgery, Keck School of Medicine, University of Southern California, Los Angeles, CA, USA

Part I

Basic Principles

Anatomy of the Sellar and Parasellar Region

1

Luigi Maria Cavallo, Domenico Solari, Alessandro Villa, Teresa Somma, and Paolo Cappabianca

1.1 Introduction

The skull base is one of the most complex anatomical regions, incorporating many different anatomical structures. The pathology of the skull base may involve a variety of lesions, neoplastic and otherwise, whose management can be difficult. In the past, this area has been accessed by many extensive and often aesthetically disfiguring transcranial and/or transfacial approaches, including the anterior, anterolateral, and posterolateral routes.

The transsphenoidal route facilitates access to the skull base via the nose. Because of its versatility, it can be considered the least traumatic route to the sella. The transsphenoidal route provides excellent visualization of the pituitary gland and related pathology, and it offers lower morbidity and mortality than open approaches to this region [1–3]. The wider, panoramic view offered by the endoscope has propelled the development of a variety of modifications of the transsphenoidal approach targeted to the entire skull base [4–8]. Direct exposure of the suprasellar, retrosellar, and retroclival spaces can now be gained using these approaches. With the evolution of technical procedures in such critical areas reached through narrow corridors, perfect understanding and knowledge of the surgical anatomy is fundamental.

L.M. Cavallo, MD, PhD (✉) • D. Solari, MD, PhD • A. Villa, MD
T. Somma, MD • P. Cappabianca, MD
Division of Neurosurgery, Department of Neurosciences, Reproductive and Odontostomatological Sciences, Universita' degli Studi di Napoli Federico II, Naples, Italy
e-mail: lcavallo@unina.it; d.solari.md@gmail.com; alessandrovilla83@gmail.com; teresa.somma85@gmail.com; paolo.cappabianca@unina.it

1.2 Endoscopic Anatomy of the Sphenoid Sinus

The anatomy of the sphenoid sinus cavity and skull base as seen from the endoscopic endonasal point of view can be divided into four areas, according to the different surgical approaches:

- The sellar area
- The suprasellar area, explored through the transtuberculum-transplanum approach
- The parasellar area (for lesions of the cavernous sinus and Meckel's cave)
- The clival area

1.2.1 Basic Concepts

The endoscopic endonasal procedure is usually performed using a rigid 0° endoscope, 18 cm in length and 4 mm in diameter (Karl Storz Endoscopy, Tuttlingen, Germany), as the sole visualizing tool; angled scopes can be used to further explore the suprasellar area. A high-definition (HD) camera, connected to a widescreen HD monitor, guarantees excellent image quality. Dedicated surgical instruments with different angled tips are needed to permit movements in all the visible corners of the surgical field [9]. To increase the working space and the maneuverability of the instruments (above all in extended approaches), it may be advisable to perform a middle turbinectomy on one side, a middle turbinate lateral luxation in the other nostril, and removal of the posterior portion of the nasal septum. A wider anterior sphenoidotomy is recommended, especially in the lateral and superior directions, where bony spurs are flattened to create adequate space for the endoscope during the deeper steps of the procedure [5].

G. Zada et al. (eds.), *Atlas of Sellar and Parasellar Lesions: Clinical, Radiologic, and Pathologic Correlations*,
DOI 10.1007/978-3-319-22855-6_1

1.2.2 Head Positioning

The head is not placed in a neutral position. According to the target area of interest, it can be extended approximately 10–15° for anterior approaches, or it may be slightly flexed for approaches to the clivus, to facilitate the mobility of the endoscope and prevent surgical instruments from being restricted by the thorax. The surgeon works from the patient's right side.

1.3 Standard Endoscopic Endonasal Approach to the Sellar Region

The endoscope is usually introduced through one nostril, sliding along the floor of the nasal cavity following the inferior turbinate; the choana is identified, limited medially by the vomer (which is often a reliable midline marker) and superiorly by the floor of the sphenoid sinus [10, 11].

Thereafter, the middle turbinate is compressed laterally to enlarge the space between the middle turbinate and the nasal septum, and the endoscope is angled upward along the roof of the choana approximately 1.5 cm, until the sphenoid ostium is identified.

It is not always mandatory to visualize the sphenoid ostium once the choana is identified; access to the sphenoid cavity can also be achieved by ascending along the sphenoethmoidal recess for approximately 1–1.5 cm.

Thereafter, the nasal septum is detached from the sphenoid rostrum, and the anterior wall of the sphenoid sinus is enlarged circumferentially, taking care to not extend too aggressively in an inferolateral direction, where the sphenopalatine artery or its major branches lie [12].

Septa inside the sphenoid sinus should be identified and resected or carefully drilled down so that the posterior and lateral walls of the sphenoid sinus are visible, with the sellar floor at the center, the planum sphenoidale above, and the clival indentation below (Fig. 1.1). The pituitary gland is situated within the hypophyseal fossa, a fibro-osseous compartment near the center of the cranial base. This fossa is limited laterally and superiorly by reflections of dura mater and anteriorly, posteriorly, and inferiorly by the sella turcica, a depression in the body of the sphenoid bone. The sellar floor lies at the center on the posterior sphenoid sinus wall and continues above to the planum sphenoidale and below to the clivus. The optic nerve prominences, above, are formed by the bony covering of the optic nerves; the carotid prominences, below, cover the internal carotid arteries, with the opticocarotid recess in between [11, 13]. The lateral

opticocarotid recess is created by the pneumatization of the optic strut of the anterior clinoid process. Although it is rarely visible in the cavity of the sphenoid sinus, it is important to define the position of the medial opticocarotid recess, representing a key point in entering the suprasellar area [14].

Once the sellar dura is opened, the anterior lobe of the pituitary gland comes into view. Its inferior surface usually conforms to the shape of the sellar floor, but its lateral and superior margins vary in shape because these walls are composed of soft tissue rather than bone. Posteriorly, the neurohypophysis (posterior pituitary gland) can be observed and is often softer, gelatinous, and more densely adherent to the posterior sellar wall, the dorsum sellae. Above, the diaphragma sellae covers the pituitary gland, except for a small central opening through which the pituitary stalk (infundibulum) passes. Folds of dura mater, which constitute the lateral walls of the hypophyseal fossa, also comprise the medial wall of the cavernous sinuses; the internal carotid artery (ICA) coursing through the cavernous sinus can be appreciated at this level [11, 13].

The pituitary gland derives its blood supply from two major groups of arteries. The superior hypophyseal artery primarily supplies the anterior lobe, the pituitary stalk, and the inferior surface of the optic nerve and chiasm, whereas the inferior hypophyseal artery is primarily related to the pars nervosa. The superior hypophyseal artery can arise from the supraclinoid portion of the ICA or from the posterior communicating artery, whereas the inferior hypophyseal artery arises from the meningohypophyseal trunk, a branch of the cavernous segment of the ICA.

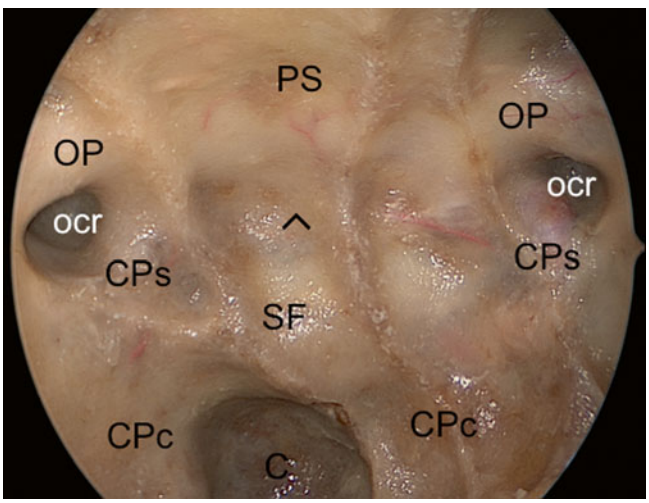

Fig. 1.1 Anatomical picture showing the posterior wall of the sphenoid sinus; all the anatomical landmarks are visible, but they may vary according to the degree of pneumatization of the sphenoid sinus. ^ tuberculum sellae as seen from the endoscopic endonasal view (recently called the "suprasellar notch"), *C* clival indentation, *CPc* paraclival segment of the carotid protuberance, *CPs* parasellar segment of the carotid protuberance, *ocr* lateral optocarotid recess, *OP* optic protuberance, *PS* planum sphenoidale, *SF* sellar floor

1.4 Extended Endoscopic Transsphenoidal Approaches

1.4.1 Suprasellar Area

The sphenoid sinus represents a window of access to the midline skull base via the endonasal corridor; when the sinus is well pneumatized, all main bony landmarks can be identified. The sellar floor occupies a central position, with the planum sphenoidale above and the clival indentation below; on both sides, lateral to the sellar floor, are the two bony prominences of the intracavernous internal carotid arteries, and the optic nerves can be identified slightly superiorly. Between these two protuberances, depending on the degree of pneumatization of the sphenoid sinus, the projection of the optic strut of the anterior clinoid process creates the lateral opticocarotid recess [7, 13–15].

Immediately above, the tuberculum sellae can be seen as an indentation represented by the angle formed by the convergence of the planum sphenoidale with the sellar floor. Recently, we renamed this structure as the "suprasellar notch" [16]. Anteriorly lies the planum sphenoidale, which is limited on both sides by the optic nerve protuberances, diverging toward the orbits.

The removal of the upper half of the sella, the tuberculum sellae, and the posterior portion of the planum sphenoidale offers the possibility of exploring and operating in the suprasellar region (Fig. 1.2). The entire suprasellar region can be divided into four intradural areas: the suprachiasmatic region, the subchiasmatic region, the retrosellar region, and the ventricular region [15].

In the suprachiasmatic region, the chiasmatic and the lamina terminalis cisterns are accessible. The anterior margin of the optic chiasm and the medial portion of the optic nerves, the anterior cerebral arteries, the anterior communicating artery, and the recurrent arteries of Heubner can be identified, together with the gyri recti of the frontal lobes [17].

In the subchiasmatic space, the pituitary stalk is encountered below the optic chiasm, with the superior hypophyseal arteries and their perforating branches supplying the inferior surface of the optic chiasm and the optic nerves (Fig. 1.3). The superior aspect of the pituitary gland and the dorsum sellae are also visible.

The retrosellar area, explored by passing with the endoscope between the pituitary stalk and the ICA above the dorsum sellae, includes the upper third of the basilar artery, the pons, the superior cerebellar arteries, the oculomotor nerves, the posterior cerebral arteries, the mammillary bodies, and the floor of the third ventricle [18, 19].

The third ventricle can be opened at the level of the tuber cinereum and the endoscope can be advanced into the ventricular cavity, obtaining a panoramic view of the ventricular

area, including the thalami and the massa intermedia, the foramina of Monro and anterior commissure anteriorly, the choroid plexus of the third ventricle, the pineal and the suprapineal recesses, the posterior commissure, the habenular commissure, the habenular trigone, and the cerebral aqueduct posteriorly.

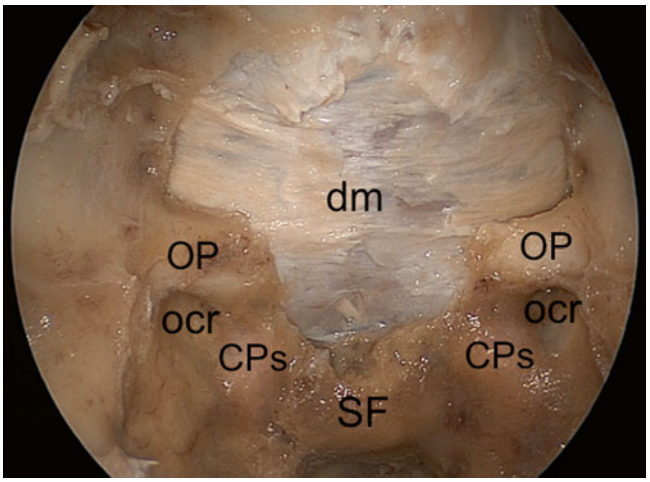

Fig. 1.2 The pattern of bony removal of the planum sphenoidale resembles a chef's hat, limited in its posterior part by the medial border of the lateral optocarotid recess (ocr) and by the bony prominence of the optic nerve. *CPc* paraclival segment of the carotid protuberance, *CPs* parasellar segment of the carotid protuberance, *dm* dura mater of the planum sphenoidale, *OP* optic protuberance, *SF* sellar floor

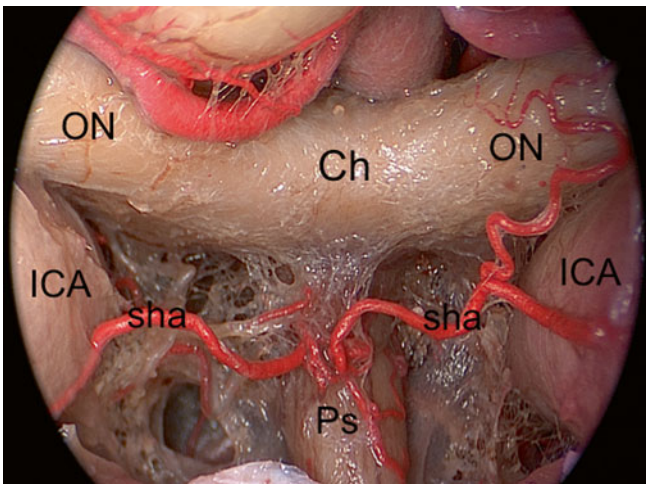

Fig. 1.3 Intradural exploration of the suprasellar area after removal of the tuberculum sellae and planum sphenoidale. *Ch* chiasm, *ICA* internal carotid artery, *ON* optic nerve, *Ps* pituitary stalk, *sha* superior hypophyseal artery

1.4.2 The Parasellar Area

The parasellar area is accessible through the lateral wall of the sphenoid sinus. The cavernous sinus apex and the trigeminal maxillary and mandibular nerve protuberances usually lie on its bony surface (Fig. 1.4). Once bone has been removed, the medial cavernous sinus wall (composed of fibrous trabecular tissue) is visualized, enclosing the C-shaped segment of the intracavernous internal carotid artery [20–23] (Fig. 1.5).

Displacing the ICA superolaterally, it is possible to visualize the meningohypophyseal trunk; the inferolateral trunk lies lateral to the carotid artery (Fig. 1.6). As seen from the endoscopic endonasal standpoint, the oculomotor nerve partially covers the trochlear nerve, whereas the V1 branch of the trigeminal nerve can be partially hidden by the sixth nerve. The oculomotor and trochlear nerves are parallel structures, coursing in a slight caudocranial direction and crossing the C-shaped ICA segment toward the superior orbital fissure. The sixth cranial nerve runs inferiorly after crossing the lower paraclival tract of the carotid artery; it usually receives sympathetic fibers from the ICA adventitia. All these nerves, together with the ophthalmic nerve, course in a slightly lateral and superior direction toward the superior orbital fissure, while the maxillary nerve runs inferiorly to reach the foramen rotundum [24] (Fig. 1.7). The oculomotor nerve, the trochlear nerve, and first two divisions of the trigeminal nerve are embedded in the lateral wall of the cavernous sinus, lying between the endothelial lining and the dura mater, whereas the abducens nerve is contained within the sinus itself. The cavernous sinus also envelops a portion of the ICA and the sympathetic nerve plexus encircling it. The intracavernous segment of the ICA extends forward, adjacent to the superolateral surface of the body of the sphenoid bone, in a groove called the carotid sulcus.

The oculomotor and abducens nerves create a triangular area whose base is represented by the lateral loop of the ICA: the outer surface of this area contains the fourth cranial nerve and a portion of V1. The abducens nerve and V2 enclose a quadrangular area, laterally limited by the bony surface of the lateral wall of the sphenoid sinus, extending from the superior orbital fissure to the foramen rotundum and medially by the ICA. Finally, an inferior quadrangular area can be identified, which is limited superiorly by V2 and inferiorly by the Vidian nerve; its anterior margin is represented by the bony surface of the lateral wall of the sphenoid sinus from the foramen rotundum to the pterygoid canal, and its posterior margin is the intrapetrous segment and the caudal portion of the ICA. This quadrangular area can be used to enter Meckel's cave [20].

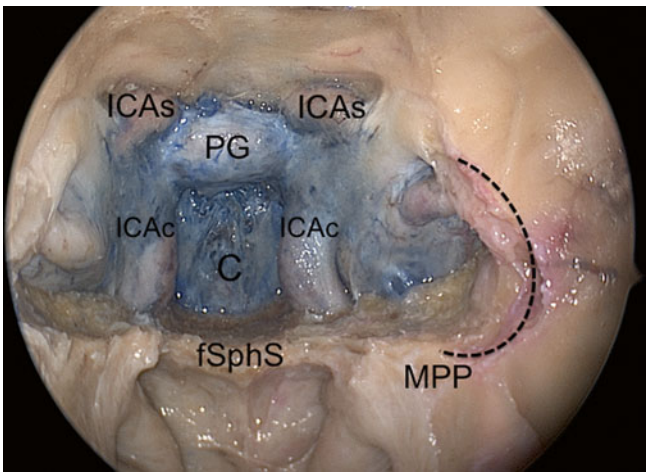

Fig. 1.4 Endoscopic view after bony removal of the sella, clivus (*C*), and the intracavernous internal carotid arteries. The medial pterygoid process has been drilled away, thus allowing a wide exposure of the lateral recess of the sphenoid sinus. The *dotted line* represents the lateral recess of the sphenoid sinus after drilling of the medial pterygoid process. *ICAc* paraclival segment of the internal carotid artery, *ICAs* parasellar segment of the internal carotid artery, *fSphS* floor of the sphenoid sinus, *MPP* medial pterygoid plate, *PG* pituitary gland

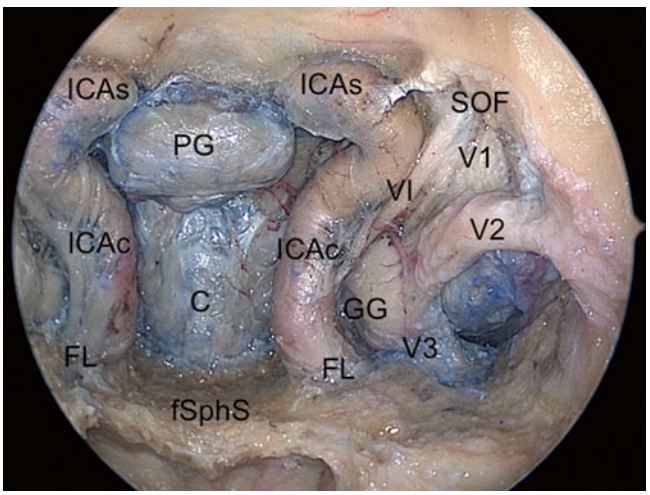

Fig. 1.5 Endoscopic view after bony removal of the lateral recess of the sphenoid sinus. *C* clivus, *ICAc* paraclival segment of the internal carotid artery, *ICAs* parasellar segment of the internal carotid artery, *FL* foramen lacerum, *fSphS* floor of the sphenoid sinus, *GG* Gasserian ganglion, *PG* pituitary gland, *SOF* superior orbital fissure, *V1* first branch of trigeminal nerve, *V2* second branch of trigeminal nerve, *V3* third branch of trigeminal nerve, *VI* abducens nerve

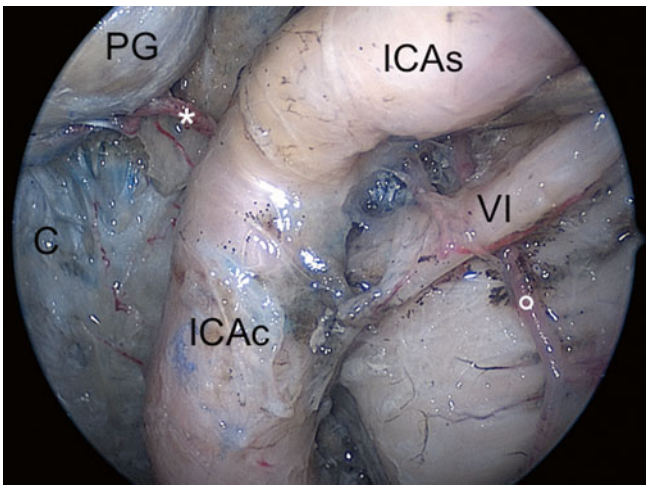

Fig. 1.6 Endoscopic close-up view of the branches of the left intracavernous internal carotid artery, including the inferior hypophyseal artery (*white asterisk*) and the inferolateral trunk (*white circle*). *C* clivus, *ICAc* paraclival segment of the internal carotid artery, *ICAs* parasellar segment of the internal carotid artery, *PG* pituitary gland, *VI* abducens nerve

1.4.3 The Clival Area

From an endonasal perspective, the clivus represents the anterior gateway to the posterior cranial fossa: two corridors can be pursued, the sphenoidal (upper clivus) and the rhinopharyngeal (lower clivus) [13, 25].

The vomer and the inferior wall of the sphenoid sinus need to be removed completely in an anteroposterior direction to allow the exposure of both the sphenoidal and rhinopharyngeal parts of the clivus (Figs. 1.6 and 1.7). The Vidian nerves, which represent the lateral limits of this exposure, can be identified lateral to the vomer-sphenoid junction [26]. These nerves, after crossing the intrapetrous carotid artery from above, reach the pterygopalatine fossa at a level inferior to that of the intrapetrous ICA. Extending posteriorly with bony removal and staying medial to these nerves, one can limit the risk of ICA injury. The lateral limit of clival bone removal is represented by the paraclival course of the intracavernous internal carotid arteries, whose bony protuberances are often clearly visible (Fig. 1.7).

Removing clival bone to the carotid protuberances, the retroclival dura harboring the basilar plexus is visualized; in the middle third of the clival area, it is possible to recognize the sixth cranial nerve entering the cavernous sinus posterior to the paraclival intracavernous carotid artery in close contact to the dorsal meningeal artery, which provides the arterial blood supply to the dura of the clival region [24] (Fig. 1.8).

Upon dural opening—performed below the vertebrobasilar junction in order to spare the sixth cranial nerve origin at the brainstem—the basilar artery and its branches, as well as the upper cranial nerves, are seen along their courses. The intradural compartment can be divided into three major regions:

- The upper third, whose main neurovascular structures are the oculomotor nerves and the posterior cerebral and superior cerebellar arteries
- The middle third, whose main landmark is represented by the sixth cranial nerves
- The lower third, including the vertebrobasilar junction, the vertebral arteries, and the ninth to twelfth cranial nerves

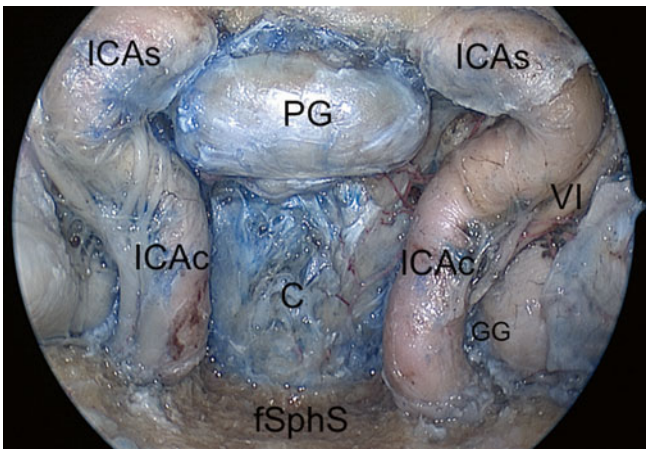

Fig. 1.7 Endoscopic view of the sellar and clival areas, enclosed between the internal carotid arteries. *C* clivus, *fSphS* floor of the sphenoid sinus, *GG* Gasserian ganglion, *ICAc* paraclival segment of the internal carotid artery, *ICAs* parasellar segment of the internal carotid artery, *PG* pituitary gland, *VI* abducens nerve

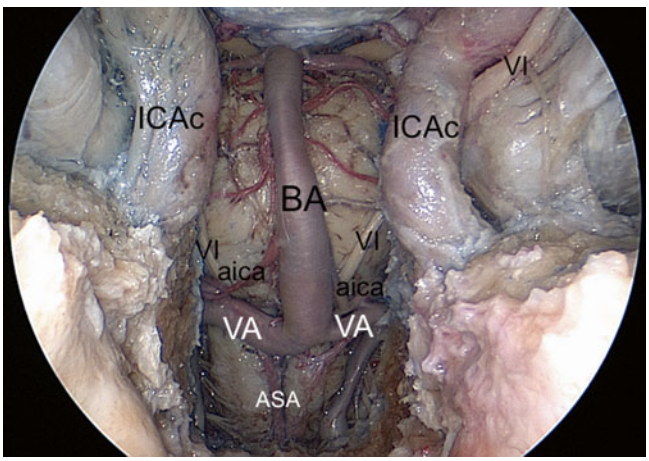

Fig. 1.8 Intradural exploration of the retroclival area after the transclival approach is extended inferiorly to C1. *AICA* anterior inferior cerebellar artery, *ASA* anterior spinal artery, *BA* basilar artery, *ICAc* paraclival segment of the internal carotid artery, *VA* vertebral artery, *VI* abducens nerve

References

1. Laws ER, Jane Jr JA. Pituitary tumors–long-term outcomes and expectations. Clin Neurosurg. 2001;48:306–19.
2. Laws ER Jr. Transsphenoidal surgery. In: Apuzzo MLJ, editor. Brain surgery: complications avoidance and management, vol. 1. New York: Churchill Livingstone; 1993. p. 357–62.
3. Weiss MH. The transnasal transsphenoidal approach. In: Apuzzo MLJ, editor. Surgery of the third ventricle. Baltimore: Williams & Wilkins; 1987. p. 476–94.
4. de Divitiis E, Cappabianca P, Cavallo LM. Endoscopic transsphenoidal approach: adaptability of the procedure to different sellar lesions. Neurosurgery. 2002;51:699–705; discussion 705–7.
5. Kassam AB, Snyderman C, Carrau RL. An evolving paradigm to the ventral skull base. Skull Base. 2004;14 Suppl 1:23.
6. Frank G, Pasquini E, Mazzatenta D. Extended transsphenoidal approach. J Neurosurg. 2001;95:917–8.
7. Cappabianca P, Cavallo LM, Esposito F, de Divitiis O, Messina A, de Divitiis E. Extended endoscopic endonasal approach to the midline skull base: the evolving role of transsphenoidal surgery. In: Pickard JD, Akalan N, Di Rocco C, et al., editors. Advances and technical standards in neurosurgery. New York: Springer; 2008. p. 152–99.
8. Laufer I, Anand VK, Schwartz TH. Endoscopic, endonasal extended transsphenoidal, transplanum transtuberculum approach for resection of suprasellar lesions. J Neurosurg. 2007;106:400–6.
9. Cappabianca P, Alfieri A, Thermes S, Buonamassa S, de Divitiis E. Instruments for endoscopic endonasal transsphenoidal surgery. Neurosurgery. 1999;45:392–5; discussion 395–6.
10. Tschabitscher M, Galzio RJ. Endoscopic anatomy along the transnasal approach to the pituitary gland and the surrounding structures. In: de Divitiis E, Cappabianca P, editors. Endoscopic endonasal transsphenoidal surgery. New York: Springer; 2003. p. 21–39.
11. Rhoton Jr AL. The sellar region. Neurosurgery. 2002;51:S335–74.
12. Cavallo LM, Solari D, Esposito F, Cappabianca P. Endoscopic endonasal approach for pituitary adenomas. Acta Neurochir (Wien). 2012;154:2251–6.
13. Cavallo LM, Messina A, Cappabianca P, Esposito F, de Divitiis E, Gardner P, Tschabitscher M. Endoscopic endonasal surgery of the midline skull base: anatomical study and clinical considerations. Neurosurg Focus. 2005;19, E2.
14. Kassam A, Snyderman CH, Mintz A, Gardner P, Carrau RL. Expanded endonasal approach: the rostrocaudal axis. Part I. Crista galli to the sella turcica. Neurosurg Focus. 2005;19(E3):1–12.
15. Cavallo LM, de Divitiis O, Aydin S, Messina A, Esposito F, Iaconetta G, et al. Extended endoscopic endonasal transsphenoidal approach to the suprasellar area: anatomic considerations–part 1. Neurosurgery. 2007;61(3 Suppl):24–33.
16. de Notaris M, Solari D, Cavallo LM, D'Enza AI, Ensenat J, Berenguer J, et al. The "suprasellar notch," or the tuberculum sellae as seen from below: definition, features, and clinical implications from an endoscopic endonasal perspective. J Neurosurg. 2012;116:622–9.
17. Rhoton Jr AL. The supratentorial arteries. Neurosurgery. 2002;51:S53–120.
18. Silva D, Attia M, Kandasamy J, Alimi M, Anand VK, Schwartz TH. Endoscopic endonasal transsphenoidal "above and below" approach to the retroinfundibular area and interpeduncular cistern-cadaveric study and case illustrations. World Neurosurg. 2014;81:374–84.
19. Kassam AB, Prevedello DM, Thomas A, Gardner P, Mintz A, Snyderman C, Carrau R. Endoscopic endonasal pituitary transposition for a transdorsum sellae approach to the interpeduncular cistern. Neurosurgery. 2008;62:57–72; discussion 72–4.
20. Cavallo LM, Cappabianca P, Galzio R, Iaconetta G, de Divitiis E, Tschabitscher M. Endoscopic transnasal approach to the cavernous sinus versus transcranial route: anatomic study. Neurosurgery. 2005;56(2 Suppl):379–89.
21. Frank G, Pasquini E. Endoscopic endonasal cavernous sinus surgery, with special reference to pituitary adenomas. Front Horm Res. 2006;34:64–82.
22. Kassam AB, Prevedello DM, Carrau RL, Snyderman CH, Gardner P, Osawa S, et al. The front door to Meckel's cave: an anteromedial corridor via expanded endoscopic endonasal approach–technical considerations and clinical series. Neurosurgery. 2009;64(3 Suppl):71–82; discussion 82–3.
23. Rhoton Jr AL. The cavernous sinus, the cavernous venous plexus, and the carotid collar. Neurosurgery. 2002;51(4 Suppl):S375–410.
24. Prevedello DM, Ditzel Filho LF, Solari D, Carrau RL, Kassam AB. Expanded endonasal approaches to middle cranial fossa and posterior fossa tumors. Neurosurg Clin N Am. 2010;21:621–35.
25. Kassam A, Snyderman CH, Mintz A, Gardner P, Carrau RL. Expanded endonasal approach: the rostrocaudal axis. Part II. Posterior clinoids to the foramen magnum. Neurosurg Focus. 2005;19, E4.
26. Kassam AB, Vescan AD, Carrau RL, Prevedello DM, Gardner P, Mintz AH, et al. Expanded endonasal approach: vidian canal as a landmark to the petrous internal carotid artery. J Neurosurg. 2008;108:177–83.

Imaging of the Sellar Region

2

Raymond Y. Huang and Srinivasan Mukundan Jr.

Imaging of the sellar and parasellar regions is clinically indicated in patients with symptoms or signs of endocrinopathy or visual field deficiency. However, a greater proportion of sellar and parasellar pathologies are often discovered incidentally as cross-sectional imaging of the brain is increasingly performed during diagnostic evaluation of unrelated neurologic problems or during staging of systemic malignancy. The latest improvements in high-resolution magnetic resonance imaging (MRI) and computed tomography (CT) techniques have greatly increased our ability to detect small sellar lesions and delineate the extent of disease prior to surgical resection. Understanding both the advantages and limitations of these imaging techniques is essential for optimizing imaging protocol and improving diagnostic accuracy.

2.1 Imaging Strategies

2.1.1 Computed Tomography (CT)

Modern CT equipment is capable of multiplanar reformation, allowing precise assessment of the bony anatomy of the sella for surgical planning. Similar to the traditional role of lateral projection of head radiographs, the shape and size of sellae are readily visualized on CT using sagittal-plane reformatted images. Moreover, with proper windowing, the pituitary gland and stalk can often be distinctly visualized apart from the cerebrospinal fluid (Fig. 2.1). While intrapituitary lesions, specifically small pituitary adenomas or cysts, are often not detectable on CT because of its less than optimal soft-tissue contrast, CT can be a useful screening test to exclude the presence of large sellar lesions, especially those that extend out of the sella causing visual field symptoms, particularly if MRI is contraindicated.

In evaluating sellar lesions, CT has an advantage over MRI because of its superior capability in visualizing bony detail and calcifications. For example, pituitary adenomas often grow slowly, allowing time for bone remodeling that is evident by demonstration of smooth cortical margins (Fig. 2.2). In contrast, an aggressive process such as a malignancy or infection can permeate or erode the bone, resulting in indistinct cortical margins. CT is also sensitive to the presence of soft-tissue calcifications that are uniquely found in a subset of sellar pathology, including vascular aneurysm, germ cell neoplasm, and craniopharyngioma. Finally, CT angiography can be helpful in confirming the presence of aneurysms that may mimic pituitary pathology and can demonstrate the spatial relationship between sellar lesions and adjacent intracranial arteries during preoperative planning.

R.Y. Huang, MD, PhD • S. Mukundan Jr., MD, PhD (✉)
Department of Radiology, Brigham and Women's Hospital,
Boston, MA, USA
e-mail: ryhuang@partners.org; smukundan@partners.org

G. Zada et al. (eds.), *Atlas of Sellar and Parasellar Lesions: Clinical, Radiologic, and Pathologic Correlations*,
DOI 10.1007/978-3-319-22855-6_2

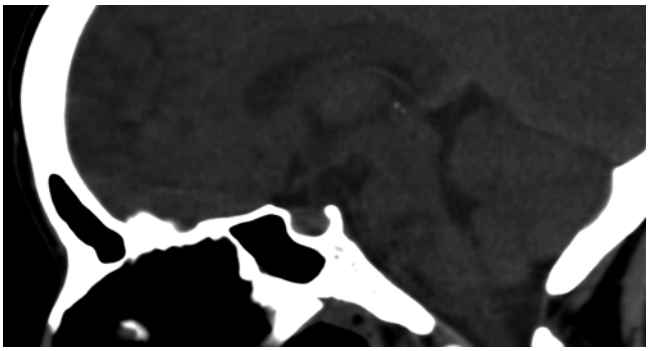

Fig. 2.1 CT image in sagittal-plane reformation shows the shape and size of the sella, with the pituitary gland and stalk clearly visualized

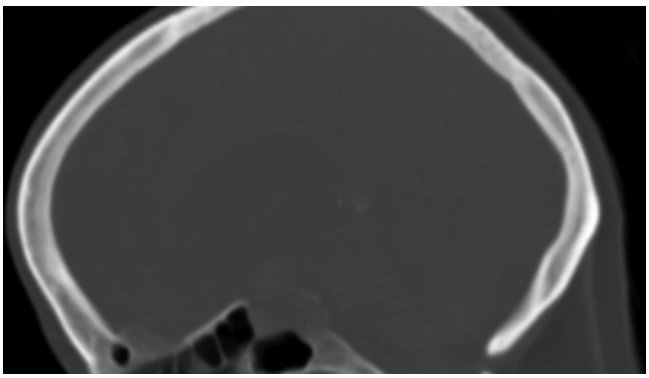

Fig. 2.2 Sagittal-plane CT image in bone window shows smooth expansion of the sella caused by a pituitary macroadenoma

2.1.1.1 Magnetic Resonance Imaging (MRI)

Because of its exquisite soft-tissue contrast and lack of ionizing radiation, MRI is the imaging modality of choice for evaluation of sellar and parasellar pathology. Because the dimensions of the sella turcica are approximately 10×10×10 mm for normal adults, an inter-slice thickness of smaller or equal to 3 mm (without gap) is needed to generate at least 3 slices through the content of the sella (Fig. 2.3). When the sella is imaged in coronal and sagittal planes at 3-mm inter-slice thickness, lesions larger than 3 mm should be detectable on both planes. The multiplanar capability of MRI not only allows initial diagnosis of sellar pathology but also facilitates preoperative planning and posttreatment surveillance for recurrence.

Although noncontrast-enhanced MRI can detect and characterize sellar pathology larger than the normal gland, small adenomas often exhibit image contrast nearly identical to the surrounding pituitary gland unless the lesions contain fluid or proteinaceous or hemorrhagic material. The standard pituitary protocol used in our institution includes sagittal and coronal T1-weighted spin-echo sequences through the sella using a small field of view (20×25 cm), thin slices (3 mm), and a high-resolution matrix (256×512), performed both before and following intravenous gadolinium administration. The protocol also includes 0.5-mm volumetric 3D T2-weighted steady-state free precession (T2 SSFP) sequence (e.g., FIESTA, CISS, etc.) in the sagittal plane through the sella, whole-brain axial fluid-attenuated inversion recovery (FLAIR), diffusion-weighted imaging (DWI), and postgadolinium volumetric 3D T1-weighted sequence (e.g., MPRAGE or SPGR). The whole-brain 3D volumetric postgadolinium sequence provides lesion coregistration to surgical guidance software and also allows confirmation of small lesions (equal to or smaller than 3 mm) occasionally observed only on one of the two 3-mm spin-echo imaging planes. In our experience, this protocol could identify a majority of sellar/parasellar pathology, greatly reducing the need to perform repeated evaluations for small adenomas using dynamic gadolinium-enhanced MRI.

For detection of small pituitary adenomas that are not apparent on delayed contrast-enhanced MRI, dynamic contrast MRI can be performed to increase lesion-to-gland contrast based on different contrast wash-in and wash-out properties between adenomas and pituitary tissues. Immediately following an intravenous bolus injection of gadolinium (0.05 mmol/kg), six sequential sets of three images are acquired every 10 s using a three-dimensional Fourier transformation gradient echo or fast turbo spin-echo sequence. For a normal pituitary gland, the stalk and posterior part of the gland enhance first because of their direct arterial supply, followed by the anterior part of the gland that receives blood from the hypophyseal-portal system. The entire gland enhances homogeneously between 30 and 60 s. The maximal

difference in the degree of enhancement between the normal pituitary tissue and adenomas often occurs during 30–60 s after the contrast administration, with the majority of adenomas appearing relatively hypoenhancing relative to the avidly enhancing pituitary gland. After 60 s, the contrast medium within the pituitary gland begins to wash out, but the adenomas often continue to take up contrast; peak enhancement occurs up to 200 s [1]. As a result, the imaging contrast between the adenoma and the pituitary tissue reduces after reaching maximum enhancement and can become reversed, with adenomas appearing more hyperintense compared with the pituitary gland on delayed imaging [2]. Some adenomas may enhance very early following contrast administration, possibly secondary to direct arterial supply, and dynamic contrast MRI can identify these adenomas as hyperintense lesions during the earliest time points [3].

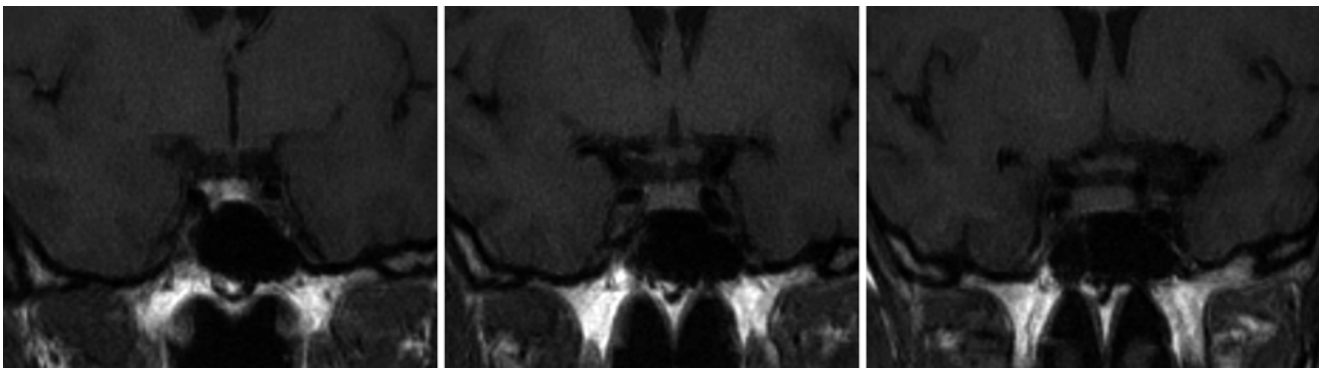

Fig. 2.3 Three consecutive coronal-plane T1-weighted images through the sella demonstrate a normal sized pituitary gland. The image on the left shows T1 shortening within the posterior pituitary